JOURNAL OF PETROLOGY | VOLUME 00 | NUMBER 0 | PAGES 1–20 | 2008 | doi:10.1093/petrology/egn049

Two Distinctive Granite Suites in the SW Bohemian Massif and their Record of Emplacement: Constraints from Geochemistry and Zircon $^{207}Pb/^{206}Pb$ Chronology

W. SIEBEL[1]*, C. K. SHANG[1], E. REITTER[1], J. ROHRMÜLLER[2] AND K. BREITER[3]

[1]INSTITUTE OF GEOSCIENCES, UNIVERSITY OF TÜBINGEN, 72074 TÜBINGEN, GERMANY

[2]BAYERISCHES LANDESAMT FÜR UMWELT, 95615 MARKTREDWITZ, GERMANY

[3]CZECH GEOLOGICAL SURVEY, 15200 PRAGUE 5, CZECH REPUBLIC

RECEIVED FEBRUARY 15, 2008; ACCEPTED SEPTEMBER 15, 2008

Various types of gneisses, migmatites and granites dominate the outcrops of the Bavarian Forest, in the southwestern Moldanubian Sector of the Bohemian Massif, providing evidence for the geological characteristics of a crustal root zone. Fourteen granite intrusions from this area have been dated by the single-zircon Pb-evaporation technique. Major and trace elements, and Rb–Sr and Sm–Nd isotope compositions of these rocks have also been determined. The $^{207}Pb/^{206}Pb$ single-zircon ages indicate Carboniferous magma production in only a few million years. The intrusions NE of the Bavarian Pfahl Zone are dated between 328 and 321 Ma, whereas ages between 324 and 321 Ma are obtained in the area SW of this zone. The coincidence between these ages and regional peak-metamorphism in this area ('Bavarian Phase') indicates a connection between metamorphism and melt extraction. When the geochemical and isotopic compositions of the granites are examined, supplemented by data from previous geochemical studies, it becomes evident that the Bavarian Pfahl Zone, which runs diagonally across the Bavarian Forest, is a terrane boundary that separates two regions of peraluminous S-type plutons predominantly of crustal anatectic origin but with distinct compositional features. Plutons located in the SW and along the Pfahl Zone (Bavarian Terrane) define a high Ca–Sr–Y suite, whereas plutons from the NE and neighbouring crystalline units (Ostrong Terrane) constitute a low Ca–Sr–Y suite. Granites from the Bavarian Terrane have significantly more radiogenic initial Nd and less radiogenic initial Sr isotope ratios than granites from the Ostrong Terrane, indicative of different source materials. These findings support the idea that the difference in magma composition is linked to the nature of the underlying crust.

KEY WORDS: *Bavarian Forest; geochemistry; granite; Pb evaporation; zircon*

INTRODUCTION

The origin and evolution of granites is a major focus of petrological research. Some of the fundamental aspects of granite petrogenesis include the identification of source components (e.g. mantle, crust or mixtures of both) and granite types. Tackling granite petrogenesis often involves radiometric age-dating (providing the time of emplacement or cooling) as well as geochemical or isotopic fingerprinting. Two key questions are: (1) Was magma formation and emplacement of short (discrete) or long (continuous) duration? (2) Do the granitoids belong to the same or different magmatic suites? In this study we investigate late Variscan S-type granites from the southwestern Moldanubian Sector of the Bohemian Massif, in the Bavarian Forest. Prior to this study the crystallization ages of these granites were largely unknown and the age relations between different intrusions of the same pluton were solely based on field observations. Moreover, existing geochemical and isotopic data were insufficient to determine the characteristic compositional

*Corresponding author. Telephone: ++49-7071-29 74 991. Fax: ++49-7071-29 57 13. E-mail: wolfgang.siebel@uni-tuebingen.de

features of the granites and to facilitate possible regional correlations.

For radiometric dating we applied the single-grain Pb-evaporation method, the principles of which were summarized by Kober (1986, 1987). The potential of this method was validated in a number of subsequent studies (Cocherie *et al.*, 1992; Chapman & Roddick, 1994; Karabinos, 1997; Klötzli, 1997; Dougherty-Page & Bartlett, 1999). As it is not possible to obtain information on the U–Pb systematics of the sample, the evaporation method is based on the premise that concordant lead is released from the sample and that discordant lead is driven out during pre-heating steps. The evaporation method has proven to provide $^{207}Pb/^{206}Pb$ zircon ages with high analytical precision (<1 % age error) that often are concordant with ages derived by other methods (e.g. Affaton *et al.*, 2000; Kröner *et al.*, 2001; Siebel *et al.*, 2003; Görz *et al.*, 2004). In a number of cases the results are compromised by zircon inheritance, and thus age significance can be attached only to ages defined by several overlapping analyses. In spite of the problem of zircon inheritance, the results of the present study reveal a single period of granite formation and, combined with previously published data, they demonstrate the intimate link of the granites with late Variscan regional crustal anatexis.

Hitherto, the granites *sensu stricto* of the Bavarian Forest have been treated as a more or less coherent group of crustally derived rocks (e.g. Holub *et al.*, 1995). It was frequently stated that certain granite massifs (Kristallgranite, Finsterau) have textural and mineralogical similarities to the Weinsberg-type granite, a coarse-grained biotite granite of the South Bohemian Batholith, Upper Austria, whereas others (Dreisessel–Plöckenstein) resemble the two-mica Eisgarn-type granite (Thiele & Fuchs, 1965). In this study we demonstrate that the granites on both sides of the Pfahl Zone have distinct compositional characteristics, which are most compatible with their derivation from two different basement-terrane units.

GEOLOGICAL SETTING AND PREVIOUS GEOCHRONOLOGY

The Bavarian Forest is located in the southwestern Bohemian Massif (Fig. 1) and forms part of the innermost zone of the Variscan orogenic belt in central Europe. It is mainly made up of migmatites, diatexites and gneisses (Teipel *et al.*, 2004, and references therein). The region belongs to the Moldanubian Sector, which is of (peri-)Gondwanan origin (Winchester *et al.*, 2002, and references therein). Together with other Gondwana-derived terranes (e.g. Armorica, Saxothuringia, Teplá–Barrandia, Moravo-Silesia), Moldanubia was accreted to the northerly situated Laurentia–Baltica during the Variscan orogeny (Devonian–Carboniferous). After final collision and amalgamation of Laurentia–Baltica, Gondwana and intervening basement fragments, the Moldanubian Sector, as the internal domain of this mountain chain, was affected by late Variscan regional metamorphism and crustal anatexis. During this event, large volumes of peraluminous S-type granites and, in places, minor volumes of I-type granites (dioritic to tonalitic rocks) were generated and intruded the metamorphosed Variscan crust.

The Moldanubian Sector does not form a coherent basement domain. It consists of different units or terranes with different structural and metamorphic evolution (Fiala *et al.*, 1995). The basement of the Bavarian Forest has often been referred to as the strongly overprinted southwestern margin of the Moldanubian. Fuchs (1976) coined the term 'Bavarikum' for this zone, and the term 'Bavarian Phase' was used by Finger *et al.* (2007) to distinguish it from the area further to the NE. In the Bavarian part of the Moldanubian sector the approximately NW–SE dextral strike-slip Pfahl Shear Zone divides the area into the 'Vorderer Bayerischer Wald' and the 'Hinterer Bayerischer Wald'. The names Bavarian Terrane and Ostrong Terrane were used by Fiala *et al.* (1995) for the areas SW and NE of the Pfahl Zone, respectively. The term 'terrane' was applied to discriminate Moldanubian basement units with different geological history separated by major thrusts or faults (Fiala *et al.*, 1995). According to this subdivision the Bavarian Terrane comprises the 'Vorderer Bayerischer Wald', whereas the Ostrong Terrane includes the 'Hinterer Bayerischer Wald' and Moldanubian rocks further NE in the Southern Palatinate Forest (Fig. 1), in the Czech Republic and in Upper Austria. For a more detailed discussion of the subdivision of the Moldanubian Sector of the Bohemian Massif, the reader is referred to Fiala *et al.* (1995) and Finger *et al.* (2007).

Lithologically, most of the Bavarian Terrane consists of various types of para-anatexites (pearl gneisses, diatexites and migmatites) and, to a minor extent, ortho-anatexites. These rocks represent a deep crustal level of the Moldanubian Sector. A higher crustal level, with cordierite-bearing gneisses, biotite–sillimanite gneisses and mica schists is exposed in the Ostrong Terrane. All these rocks re-equilibrated under low-pressure and high-temperature conditions. Calculation of the peak P–T conditions prevailing during late Variscan regional metamorphism and crustal anatexis yielded 800–850°C and 0·5–0·7 GPa (Kalt *et al.*, 1999). The metamorphic peak has been dated at 323–326 Ma by U–Pb zircon and monazite methods (Kalt *et al.*, 2000).

In general, the plutons in the Bavarian Forest are composite bodies that were formed during multiple intrusion events. Until recently, only a limited number of robust or high-resolution age determinations have been made for these rocks. A recent review of existing data was given by Klein *et al.* (2008). If older, less reliable Rb–Sr whole-rock data are excluded, the granites *senso stricto* investigated so far (i.e. Kristallgranite, Fürstenstein Pluton, Hauzenberg Pluton, Rinchnach Granite, Patersdorf Granite) yield

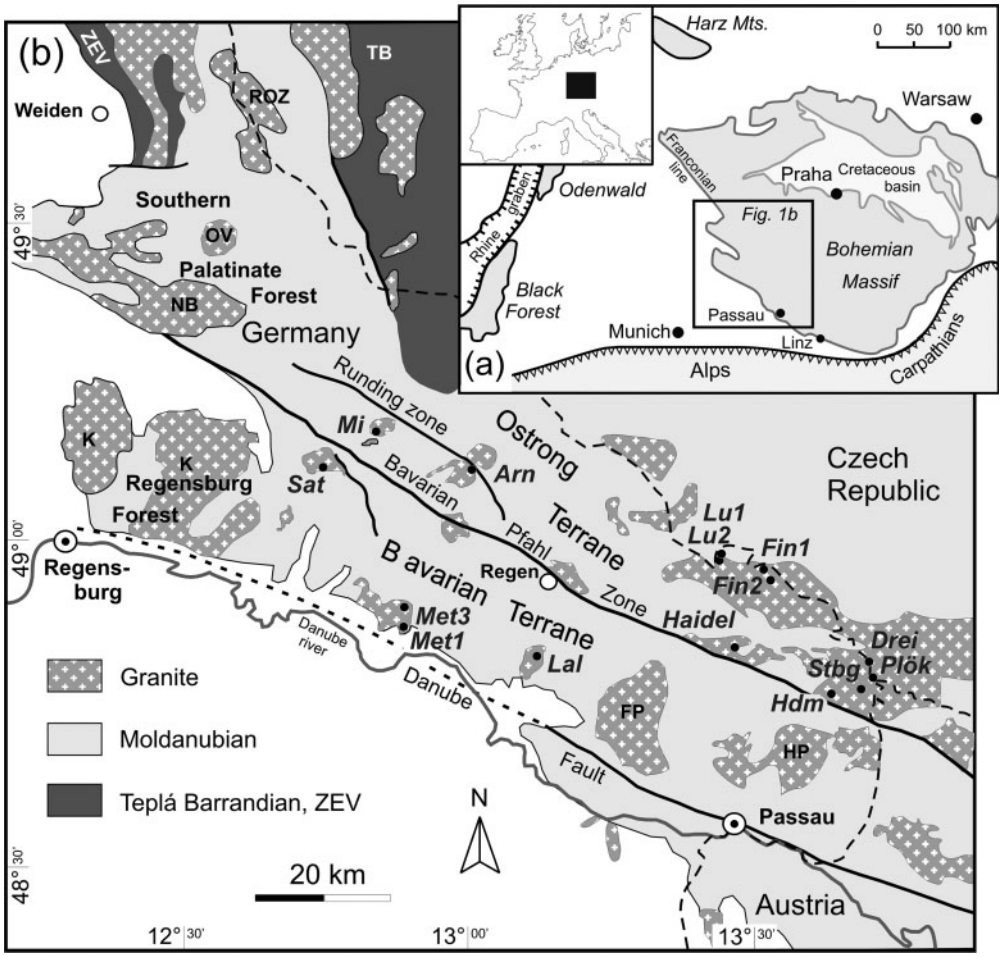

Fig. 1. (a) Map showing the location of the Bohemian Massif and neighbouring Variscan basement units situated north of the Alpine–Carpathian Mountain Belt. (b) Generalized geological map (modified after Teipel *et al.*, 2008; Klein *et al.*, 2008) showing the study area with distribution of granite intrusive rocks and sample localities (sample names in italics). Labelled plutons are those for which geochronological data were available before this study: FP, Fürstenstein Pluton; HP, Hauzenberg Pluton; K, Kristallgranite; NB, Neunburg Granite; OV, Oberviechtach Granite; ROZ, Rozvadov Pluton. The Bavarian Pfahl Zone separates the area into a southwestern (Bavarian) and northeastern (Ostrong) Terrane (for terrane subdivision see also Fig. 10). Unshaded regions are post-Variscan cover sequences. TB, Teplá–Barrandia; ZEV, Zone of Erbendorf–Vohenstrauß.

crystallization ages between 329 and 312 Ma [U–Pb or Pb–Pb ages on zircon and monazite; see Klein *et al.* (2008) for compilation].

GRANITES OF THE BAVARIAN FOREST

Post-kinematic granite intrusions occur throughout the Bavarian Forest and, at the current level of exposure, cover *c.* 1000 km^2 (Fig. 1). Most of the intrusions have sharp discordant intrusive contacts with the metamorphic country rocks and with other intrusions. However, some granite bodies, such as the Kristallgranite, remained in the migmatite zone and are arguably parautochthonous (Propach, 1989). Because of the lack of exposure, the exact contact relationships often remain unclear.

Bavarian Terrane

Isotopic characteristics and emplacement ages of the three largest plutons within the Bavarian Terrane (Kristallgranite, Fürstenstein, Hauzenberg) were reported in earlier studies (Propach *et al.*, 2000; Chen & Siebel, 2004; Klein *et al.*, 2008). The coarse-grained Kristallgranite with megacrystic K-feldspar is a widespread (~400 km^2) magmatic rock in the Regensburg Forest (Fig. 1). The Fürstenstein Pluton (~100 km^2) shows a considerable compositional variation from quartz-diorite or tonalite through medium-grained biotite granite to coarse-grained porphyritic two-mica granite. The Hauzenberg Pluton (100 km^2) comprises fine- and medium-grained biotite–muscovite granite (Hauzenberg I, Hauzenberg II) and a granodiorite intrusion, mapped and described in detail by Dollinger (1967).

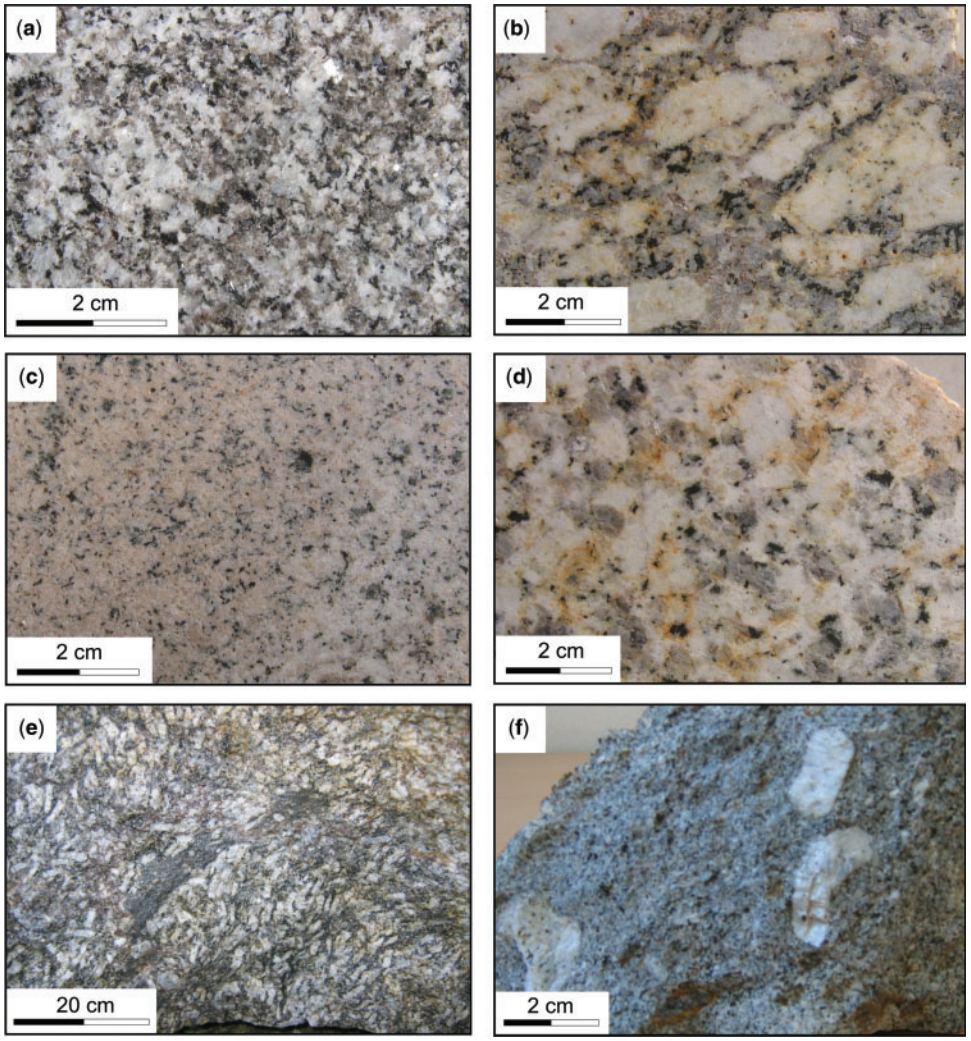

Fig. 2. Granite types and magmatic fabrics in the Bavarian Forest SW of the Pfahl Zone (Bavarian Terrane): (a) Metten Granite, medium-grained Metten facies. NE of Bavarian Pfahl Zone (Ostrong Terrane): (b) Finsterau I Granite, coarse-grained porphyritic; (c) Lusen Granite, fine-grained; (d) Plöckenstein Granite, coarse-grained two-mica granite; (e) Steinberg Granite, hiatal porphyritic with strongly aligned K-feldspar phenocrysts; (f) Haidel Granite, fine-grained, with individual K-feldspar phenocrysts.

From the Bavarian Terrane we sampled the granites of Lalling, Metten and Sattelpeilnstein (samples Lal, Met and Sat in Fig. 1). These granites comprise fine- to medium-grained varieties (Fig. 2a). The sample from the Lalling Granite (Lal) was collected from a quarry where granite is associated with small volumes of dioritic or tonalitic intrusions. The sample comprises a non-porphyritic, fine- to medium-grained biotite-granite. The Metten Pluton, located close to the Danube Fault, is the largest investigated intrusion of the Bavarian Terrane. The pluton was mapped and subdivided by Schreyer (1967) into five facies, each representing a different intrusion. According to Schreyer's classification, analysed samples comprise the medium-grained Metten facies (Met1, Fig. 2a) and the fine-grained (younger) Luhof facies (Met3). Granites with very similar texture and mineral composition crop out adjacent to the Bavarian Pfahl (Rinchnach Granite, Patersdorf Granite) and were investigated in an earlier study (Siebel *et al.*, 2006*b*). The small intrusion of Sattelpeilnstein forms an elliptical body in the eastern Regensburg Forest. The collected sample (Sat) is a medium-grained weakly porphyritic biotite-granite.

In most granite samples from the Bavarian Terrane biotite is more abundant than muscovite. In the Lalling and Sattelpeilnstein granites, muscovite occurs only as fine- to medium-grained secondary mineral. The Met1 rock, however, is a two-mica granite in which large flakes of primary muscovite and biotite occur in almost equal modal proportions.

Ostrong Terrane

In the northern part of the Ostrong Terrane several granite stocks are exposed close to the Runding Fault (Fig. 1). Amongst them, the two largest intrusions, hereafter referred to as Miltach and Arnbruck Granite, were sampled for geochemical and isotopic analyses. Both granites are leucogranites with indistinguishable textural characteristics and are composed of quartz, plagioclase, K-feldspar, biotite and muscovite. The Arnbruck Granite is cut by the Runding Fault (Fig. 1). Further SE, the large Finsterau and Dreisessel Plutons occur along the German–Czech border region. The Finsterau Pluton consists of a coarse-grained porphyritic (alkali-feldspar megacrysts) granite (Finsterau I; Fig. 2b), which dominates the outcrop area. Medium-grained, weakly porphyritic granite (Finsterau II) locally shows sharp contact against Finsterau I (Bauberger, 1981). A fine- to medium-grained two-mica granite cuts the Finsterau granites in several locations. This granite type forms a separate intrusion at and around the top of the Lusen summit and is here referred to as Lusen Granite (Fig. 2c). Samples from all these granites were chosen for analysis.

The Dreisessel–Plöckenstein Pluton, also referred to as the Plechý Pluton by Czech researchers, occupies the area SE of the Finsterau Massif. This pluton shows the most pronounced negative Bouguer gravity anomaly in the Moldanubian Sector (Blížkovský & Novotný, 1982) and modelling indicates that the pluton extends to depths greater than ~7–8 km below the present surface (Verner *et al.*, 2008). Breiter & Koller (2005) and Breiter *et al.* (2007) divided the Dreisessel–Plöckenstein Pluton into three main granite facies: (1) the generally equigranular, coarse-grained, locally weakly porphyritic Plöckenstein Granite (two-mica granite) forms the major part of the pluton (Fig. 2d); (2) serial porphyritic, coarse-grained Dreisessel Granite (two-mica granite) forms a north–south elongated body in the western part of the pluton; (3) the hiatal porphyritic Steinberg Granite [biotite-rich granite; the name is after Ott (1988, 1992)] with a medium-grained groundmass forms a crescent-shaped body SW of the Plöckenstein intrusion. The characteristic feature of the Steinberg Granite is the strong alignment of K-feldspar phenocrysts (Fig. 2e) and the high Th concentration (40–90 ppm, Breiter *et al.*, 2007). One sample of each of these granite types was taken for analysis.

Some age data for the Dreisessel–Plöckenstein Pluton have been published previously, including mineral ages in the range 319–309 Ma (Ar–Ar muscovite ages), 324–306 Ma (Rb–Sr muscovite ages) and 324–299 Ma (chemical Th–Pb monazite ages). A more complete geochronological dataset has been given by Breiter *et al.* (2007).

The southern and western parts of the Dreisessel–Plöckenstein Pluton are mainly composed of coarse-grained muscovite-rich granite that is petrographically identical to the Plöckenstein Granite. It was defined as a separate intrusion, the Haidmühle Granite, by Ott (1992) but was regarded as part of the Plöckenstein Granite by Verner *et al.* (2008). The Haidmühle Granite is bounded to the SW by the Bavarian Pfahl Zone and a change in magmatic foliation close to the Pfahl Zone is recorded by the magnetic fabric (anisotropy of magnetic susceptibility data, Verner *et al.*, 2008). A dark grey porphyritic biotite granite with K-feldspar phenocrysts (Fig. 2f) is exposed to the west of the Haidmühle Granite. This intrusion is known as the Haidel Granite (Ott, 1988). Samples from the Haidmühle Granite and the Haidel Granite were collected for analysis.

ANALYTICAL METHODS

Each granite sample (2–5 kg) was crushed and split, and *c.* 100 g representative material was pulverized in an agate mill for geochemical analysis. Major elements and certain trace elements (Ba, Y, Zr, La, Ce, Yb) were determined on fused lithium tetraborate glass beads by wavelength-dispersive X-ray fluorescence (XRF) techniques. The precision is better than 5–10% for all measured trace elements. Loss on ignition (LOI) was determined gravimetrically at 1050°C. Concentrations of Rb, Sr, Sm and Nd were determined by isotope dilution (see below). Zircons were obtained from the 200–125 and 125–63 μm sieve size fractions using a Wilfley table, a Frantz isodynamic separator and heavy liquids followed by handpicking under a binocular microscope. To study their internal structures, zircon grains were mounted in epoxy resin, polished and observed in cathodoluminescence (CL) using an electron microscope (type LEO 1459). For Pb-evaporation analyses zircons were embedded in a Re evaporation filament and measured using a Finnigan MAT 262 mass spectrometer equipped with a single secondary electron multiplier (SEM). The procedures have been described by Siebel *et al.* (2003). From each zircon grain three or four temperature steps were measured and the mean of the ^{204}Pb-corrected radiogenic $^{207}Pb/^{206}Pb$ ratios from all steps was calculated if the data for each of the steps were concordant within error. The age for several zircons from the same sample is given as a weighted average and the error refers to the 95% confidence level (ISOPLOT, Ludwig, 2003). Repeated measurements on natural zircons from zircon standard 91500 were performed for geologically realistic age and error treatment [some of the results have been published by Chen *et al.* (2002)].

For Rb–Sr and Sm–Nd isotope analyses, whole-rock powders were spiked with ^{150}Nd–^{149}Sm and ^{87}Rb–^{84}Sr tracer solutions (isotope dilution analyses) prior to dissolution in hydrofluoric acid at 180°C in pressure digestion bombs. Rb, Sr and the light rare earth elements were isolated from each other by standard ion exchange chromatography with a 5 ml resin bed of AG 50W-X12 (200–400 mesh). Nd and Sm were

separated on quartz columns using 1·7 ml Teflon powder coated with HDEHP, di-(2-ethylhexyl)-orthophosphoric acid, as cation exchange medium. Isotopic data were obtained in static mode on a Finnigan MAT 262 mass spectrometer. The $^{143}Nd/^{144}Nd$ ratios were normalized to $^{146}Nd/^{144}Nd = 0{\cdot}7219$, and the $^{87}Sr/^{86}Sr$ isotope ratios to $^{86}Sr/^{88}Sr = 0{\cdot}1194$. Repeated measurements of the La Jolla Nd standard ($n = 12$) gave a $^{143}Nd/^{144}Nd$ ratio of $0{\cdot}511838 \pm 13$ (errors are $\pm 2\sigma$ of the mean) and 10 analyses of the NBS 987 Sr standard yielded a mean value of $^{87}Sr/^{86}Sr = 0{\cdot}710248 \pm 0{\cdot}000012$, in good agreement with the certified values. Total procedural blanks were <90 pg for Nd and <220 pg for Sr. Two-stage depleted mantle Nd model-ages (T_{DM}) were calculated with depleted present-day parameters $^{143}Nd/^{144}Nd = 0{\cdot}513151$ and $^{147}Sm/^{144}Nd = 0{\cdot}219$ (Liew & Hofmann, 1988) and εNd values were calculated using present-day CHUR values of 0·1967 for $^{147}Sm/^{144}Nd$ (Jacobsen & Wasserburg, 1980) and 0·512638 for $^{143}Nd/^{144}Nd$ (Goldstein *et al.*, 1984).

SINGLE-ZIRCON Pb-EVAPORATION DATA

Inheritance of older zircon domains poses a general problem during Pb evaporation analyses. Such effects played a major role during this study, as all the investigated granites have S-type compositional characteristics (see Table 1 for the geochemical compositions of the investigated bulk-rock samples from which zircons were extracted). In general, grains with portions of pre-magmatic zircon fragments can be easily identified during isotopic measurement, as they normally yield increasingly higher $^{207}Pb/^{206}Pb$ ratios, or apparently older ages, for successively higher temperature steps. In such grains, the lower temperature steps yield higher proportions of Pb from magmatic rim zones, whereas in the higher temperature steps the proportion of Pb from inherited zircon cores predominates (see also Klötzli, 1999).

To obtain the intrusion age, reproducible $^{207}Pb/^{206}Pb$ ages for different temperature steps of a given grain, and consistent ages for different grains from the same sample are needed. For such measurements, an inherited zircon contribution can be largely excluded. Given the existence of pre-magmatic zircon fragments, this necessitated the analysis of a relatively large number of zircon grains (in many cases 10 or more grains per sample) to place effective constraints on granite crystallization. A summary of the data for magmatic zircons is given in Table 2.

Bavarian Terrane

Zircons from the granites belonging to the Bavarian Terrane have specific morphological features. In the Metten Pluton, zircons typically occur as near-spherical grains and show stubby crystal habits with little morphological variation. As seen in CL images (e.g. Fig. 3a and b), only a few grains show well-developed regular oscillatory growth zoning. An explanation for oscillatory zoning in zircons involves unstable chemical gradients around the grain during magmatic crystallization. Diffusion associated with late magmatic processes can obliterate the igneous oscillatory zoning pattern (Connelly, 2000). It is remarkable that some of the Metten grains are similar in appearance to those observed in high-grade gneisses (Corfu *et al.*, 2003). Such grains might represent overgrowth-free xenocrystic zircons that might have been assimilated into the magma during late-stage crystallization. Zircons from the Lalling, Sattelpeinstein and Miltach granites form elongated idiomorphic grains and show magmatic growth zonation (Fig. 3c–e). In some cases this zonation is part of an older zircon generation. Such grains can be identified if resorption zones between inner and outer zones are developed (Fig. 3d, grains 3 and 4).

The Pb-evaporation technique applied to three grains of Metten sample Met1 (Metten facies) gives ages around 322 and 328 Ma, with a mean value of $324{\cdot}2 \pm 5{\cdot}0$ Ma (Fig. 4a). Four zircon ages from sample Met3 (Luhof facies) vary between 318 and 326 Ma with a slightly younger mean age of $321{\cdot}0 \pm 3{\cdot}8$ Ma (Fig. 4b). Other grains in both samples yield increasingly radiogenic $^{207}Pb/^{206}Pb$ ratios for successively higher heating steps, indicating the presence of pre-magmatic zircon fragments. The $^{207}Pb/^{206}Pb$ ages of five zircons from Lalling sample Lal are between 315 and 329 Ma with a mean age of $321{\cdot}6 \pm 5{\cdot}6$ Ma (Fig. 4c). $^{207}Pb/^{206}Pb$ ages from this sample are more scattered than for the other samples, which can be ascribed to the higher contribution of common lead, indicated by high $^{204}Pb/^{206}Pb$ ratios observed in nearly all grains from the Lalling Granite (Table 2). Admixture of older inherited zircon material was observed in two grains that yielded increasing $^{207}Pb/^{206}Pb$ ratios as the evaporation temperature was increased from 1380°C through 1400°C and 1420°C to 1440°C. Information provided by these analyses points to a minimum age of >360 Ma for the pre-magmatic zircon component. Four grains of Sattelpeilnstein sample Sat gave ages between 319 and 327 Ma with a weighted mean age of $322{\cdot}3 \pm 3{\cdot}4$ Ma (Fig. 4d). In a fifth grain, increase of $^{207}Pb/^{206}Pb$ ratios with evaporation temperature suggests inheritance.

Ostrong Terrane

The CL images of most granites from the Ostrong Terrane have a similar appearance and zircon populations from different samples show similar internal structures. Usually, crystals are prismatic, with aspect ratios up to three, and exhibit well-preserved oscillatory growth zonation. Crystals vary in size from 400 to 200 μm in the Finsterau I Granite (Fig. 3g) and from 250–63 μm in all other granites. Many grains show oscillatory zoning with brightly luminescent centres surrounded by dark rims (e.g. grains in Figs. 3e, i and j). In some grains inner

Table 1: Major and trace element analytical data, and Rb–Sr and Sm–Nd isotope composition of granites from the Bavarian Forest

Terrane:	Bavarian Terrane				Ostrong Terrane										
Sample:	Met1	Lal	Met3	Sat	Fin I	Haidel	Stein	Plöck	Fin II	Hdm	Lu1	Lu2	Mi	Arn	Drei
Longitude (N):	48°51′	48°54′	48°48′	49°08′	48°57′	48°51′	48°47′	48°46′N	48°57′	48°47′	48°56′	48°56′	49°10′	49°07′	48°47′
Latitude (E):	12°56′	12°54′	13°07′	12°40′	13°37′	13°32′	13°47′	13°50′	13°37′	13°44′	13°30′	13°30′	12°47′	12°59′	13°48′
wt%															
SiO_2	68·38	68·72	69·91	70·74	67·54	68·88	69·55	70·26	70·28	71·96	72·02	72·17	72·55	73·61	74·24
TiO_2	0·45	0·43	0·43	0·44	0·68	0·46	0·37	0·18	0·33	0·17	0·18	0·23	0·17	0·19	0·20
Al_2O_3	15·52	14·92	15·29	14·80	15·65	15·35	15·08	15·05	15·14	14·50	14·21	14·35	14·34	14·86	13·46
Fe_2O_3	3·04	3·43	2·46	2·63	3·77	2·56	2·18	1·45	2·16	1·39	1·42	1·56	1·26	1·46	1·69
MnO	0·04	0·04	0·03	0·04	0·05	0·03	0·02	0·03	0·02	0·03	0·02	0·02	0·03	0·04	0·03
MgO	1·10	1·03	0·96	0·70	1·19	0·85	0·56	0·34	0·65	0·44	0·44	0·42	0·33	0·46	0·33
CaO	1·32	1·82	1·99	1·00	2·24	1·11	0·65	0·54	0·87	0·52	0·64	1·09	0·62	0·66	0·45
Na_2O	3·29	3·30	3·45	3·09	3·54	2·91	2·86	3·19	3·07	2·77	3·02	3·30	3·43	3·47	2·92
K_2O	5·03	4·68	4·65	5·48	4·10	6·04	6·33	5·66	5·26	5·79	6·26	5·29	4·83	4·87	4·32
P_2O_5	0·18	0·16	0·21	0·30	0·25	0·25	0·30	0·29	0·27	0·25	0·18	0·17	0·30	0·33	0·28
LOI	0·65	0·32	0·45	0·52	0·99	0·71	1·07	1·12	1·21	1·20	0·85	0·53	0·53	0·89	1·30
Total	99·1	99·0	100·0	99·9	100·2	99·3	99·1	98·2	99·4	99·1	99·3	99·34	98·5	100·9	99·3
ppm															
Ba	629	794	807	436	918	709	394	224	406	316	472	1230	212	222	80
Rb	265	176	225	345	228	304	438	388	279	275	213	175	336	370	471
Sr	160	333	182	95	188	133	59	34	87	69	94	165	47	77	29
Y	7	11	18	26	23	13	9	4	15	6	4	6	10	11	7
Zr	104	123	197	250	275	211	185	67	162	69	86	100	70	75	76
La	22	33	39	38	53	57	43	17	40	11	19	20	13	16	15
Ce	48	67	90	94	133	148	128	54	97	33	45	55	—	—	34
Nd	20·6	35·2	34·6	38·5	57·5	73·2	74·9	22·5	42·5	13·7	18	23·7	13·6	14·49	26·4
Sm	3·97	6·43	6·51	7·69	9·59	12·66	13·0	5·13	8·78	3·29	4·4	4·27	3·38	3·48	5·62
Yb	0·8	1·0	1·6	2·3	2·1	1·4	1·3	1·3	1·9	1·2	0·9	1·0	1·3	1·4	1·6
A/CNK	1·17	1·08	1·07	1·15	1·09	1·15	1·18	1·22	1·23	1·23	1·10	1·09	1·20	1·22	1·31
$^{87}Rb/^{86}Sr$	4·783	1·528	3·595	10·56	3·525	6·626	21·73	33·96	9·37	11·70	x	3·071	21·12	14·05	47·67
$^{87}Sr/^{86}Sr$	0·728500	0·712861	0·723500	0·754269	0·724469	0·742012	0·809087	0·860844	0·752326	0·765084	x	0·723241	0·803710	0·794821	0·919617
Error	10	7	10	9	10	9	10	10	8	10	x	11	10	9	10
$^{87}Sr/^{86}Sr(i)$	0·70645	0·70586	0·70708	0·70585	0·70811	0·71155	0·70766	0·7038*	0·70910	0·71165	x	0·70904	0·70724	0·72981	0·6977*
$^{147}Sm/^{144}Nd$	0·1171	0·1110	0·1144	0·1214	0·1008	0·1046	0·1046	0·1379	0·1248	0·1455	x	0·1090	0·1507	0·1452	0·1286
$^{143}Nd/^{144}Nd$	0·512168	0·512258	0·512196	0·512174	0·512149	0·512022	0·512027	0·512108	0·512109	0·512114	x	0·512125	0·512121	0·512115	0·512072
Error	8	8	10	10	12	10	9	7	12	9	x	10	10	9	8
$^{143}Nd/^{144}Nd(i)$	0·511920	0·512024	0·511956	0·511918	0·511934	0·511801	0·511802	0·511815	0·511844	0·511808	x	0·511893	0·511804	0·511806	0·511797
$\varepsilon Nd(t)$	−5·9	−3·9	−5·3	−6·0	−5·6	−8·2	−8·1	−7·9	−7·4	−8·1	x	−6·4	−8·2	−8·1	−8·2
T_{DM} (Ga)	1·55	1·38	1·49	1·55	1·52	1·74	1·73	1·71	1·67	1·73	x	1·59	1·73	1·73	1·74

Major and trace elements were determined by XRF, except for Rb, Sr, Sm and Nd, which were determined by isotope dilution technique. LOI, loss on ignition; —, below detection limit; x, not analyzed; errors ($2\sigma_m$, for $^{87}Sr/^{86}Sr$ and $^{143}Nd/^{144}Nd$ ratios) refer to the last digits. T_{DM}, two-stage depleted mantle Nd model-age.

*Overcorrected initial Sr isotope ratio as suggested by high $^{87}Rb/^{86}Sr$ ratio of this sample (possibly caused by post-crystallization alteration).

Table 2: $^{207}Pb/^{206}Pb$ single zircon evaporation data from granites from the Bavarian Forest

Sample	No.[1]	$^{204}Pb/^{206}Pb$	$^{206}Pb^*/^{208}Pb^*$	Th/U[2]	$^{207}Pb^*/^{206}Pb^*$[3]	Age (Ma)	Error (Ma)[4]
Bavarian Terrane							
Lalling Granite							
Lal_3	174	0·001292	10	0·31	0·052691 ± 0·000060	315·5	3·5
Lal_5	334	0·001213	62	0·05	0·052900 ± 0·000043	324·5	3·0
Lal_7	141	0·001723	12	0·26	0·052672 ± 0·000054	314·8	3·3
Lal_9	183	0·000198	22	0·14	0·052997 ± 0·000052	328·7	3·2
Lal_11	176	0·000203	8·5	0·37	0·052899 ± 0·000055	324·5	3·3
Weighted av.						**321·6**	**5·6**
Metten Granite							
Met3_1	238	0·000065	159	0·02	0·052743 ± 0·000043	317·8	3·0
Met3_7	257	0·000068	33	0·10	0·052783 ± 0·000027	319·5	2·6
Met3_8	66	0·000193	64	0·05	0·052827 ± 0·000106	321·4	5·1
Met3_10	424	0·000080	29	0·11	0·052925 ± 0·000037	325·6	3·0
Weighted av.						**321·0**	**3·8**
Met1_1	117	0·000177	181	0·02	0·052855 ± 0·000109	322·6	5·2
Met1_6	393	0·000282	15	0·21	0·052982 ± 0·000044	328·1	3·0
Met1_8	174	0·000071	64	0·05	0·052832 ± 0·000032	321·6	2·6
Weighted av.						**324·2**	**5·0**
Sattelpeilnstein Granite							
Sat_1	345	0·000035	59	0·05	0·052849 ± 0·000039	322·4	2·9
Sat_2	263	0·000029	44	0·07	0·052831 ± 0·000039	321·6	2·8
Sat_3	351	0·000250	8·7	0·37	0·052777 ± 0·000046	319·3	3·0
Sat_4	116	0·000025	72	0·04	0·052964 ± 0·000057	327·3	3·4
Weighted av.						**322·3**	**3·4**
Ostrong Terrane							
Miltach Granite							
Mi_1	402	0·000110	39	0·08	0·052794 ± 0·000033	320·0	2·7
Mi_3	147	0·000163	381	0·01	0·052767 ± 0·000027	318·8	2·6
Mi_4	440	0·000063	59	0·05	0·052843 ± 0·000025	322·1	2·5
Mi_5	249	0·000160	15	0·22	0·052966 ± 0·000073	327·4	3·9
Weighted av.						**321·8**	**3·7**
Arnbruck Granite							
Arn_3	322	0·000374	12	0·25	0·052921 ± 0·000047	325·4	3·1
Arn_5	177	0·000086	20	0·15	0·052914 ± 0·000071	325·2	2·9
Weighted av.						**325·3**	**2·1**
Lusen Granite							
Lu1_1	295	0·000120	55	0·06	0·052867 ± 0·000062	323·1	3·5
Lu2_1	360	0·000157	33	0·10	0·052923 ± 0·000039	325·5	2·8
Lu2_2	259	0·000198	28	0·11	0·052987 ± 0·000044	328·3	3·0
Lu2_4	187	0·000031	78	0·04	0·052921 ± 0·000042	325·4	2·9
Lu2_5	218	0·000048	71	0·05	0·052805 ± 0·000025	320·5	2·6
Weighted av. Sample Lu2						**324·9**	**3·5**

(continued)

Table 2: Continued

Sample	No.[1]	$^{204}Pb/^{206}Pb$	$^{206}Pb^*/^{208}Pb^*$	Th/U[2]	$^{207}Pb^*/^{206}Pb^*$[3]	Age (Ma)	Error (Ma)[4]
Finsterau II Granite							
Fin II_1	89	0·000130	27	0·12	0·052875 ± 0·000068	323·5	3·7
Fin II_2	477	0·000100	52	0·06	0·052844 ± 0·000049	322·2	3·1
Fin II_3	271	0·000038	30	0·11	0·052828 ± 0·000033	321·4	2·7
Fin II_4	367	0·000029	31	0·10	0·052905 ± 0·000029	324·8	2·6
Fin II_5	367	0·000149	30	0·11	0·052919 ± 0·000039	325·4	2·8
Fin II_6	471	0·000061	57	0·06	0·052955 ± 0·000026	326·9	2·6
Weighted av.						**324·1**	**1·8**
Finsterau I Granite							
Fin I_1	411	0·000062	21	0·15	0·052902 ± 0·000030	324·6	2·6
Fin I_2	313	0·000070	28	0·11	0·052918 ± 0·000049	325·3	3·1
Fin I_3	367	0·000162	25	0·13	0·052912 ± 0·000028	325·1	2·6
Fin I_4	376	0·000148	32	0·10	0·052909 ± 0·000040	324·9	2·9
Fin I_7	588	0·000040	29	0·11	0·053005 ± 0·000018	329·1	2·4
Weighted av.						**325·9**	**1·9**
Haidmühle Granite							
Hdm_6	353	0·000036	31	0·10	0·052807 ± 0·000027	320·6	2·6
Hdm_10	226	0·000014	44	0·07	0·052816 ± 0·000027	320·9	2·6
Hdm_15	206	0·000062	21	0·15	0·052808 ± 0·000054	320·6	3·3
Weighted av.						**320·7**	**1·6**
Haidel Granite							
Haidel_1	253	0·000012	19	0·17	0·052916 ± 0·000046	325·2	3·0
Haidel_4	359	0·000022	17	0·06	0·052929 ± 0·000027	325·8	2·6
Haidel_6	186	0·000071	28	0·11	0·052842 ± 0·000029	322·0	2·6
Haidel_8	193	0·000058	15	0·21	0·052808 ± 0·000042	320·6	2·9
Weighted av.						**323·4**	**2·6**
Plöckenstein Granite							
Plök_1	224	0·000048	70	0·05	0·052805 ± 0·000025	320·5	2·6
Plök_3	326	0·000140	26	0·12	0·052977 ± 0·000040	327·8	2·9
Plök_4	182	0·000044	48	0·07	0·052910 ± 0·000055	325·0	3·3
Plök_5	300	0·000065	7·8	0·41	0·052936 ± 0·000042	326·1	2·9
Weighted av.						**324·8**	**3·4**
Dreisessel Granite							
Drei_1	215	0·000211	8·8	0·36	0·052958 ± 0·000074	327·0	3·9
Drei_2	308	0·000149	14	0·23	0·052968 ± 0·000059	327·5	3·4
Drei_3	185	0·000110	8·9	0·36	0·052955 ± 0·000048	326·9	3·1
Weighted av.						**327·1**	**1·9**
Steinberg Granite							
Stein_2	329	0·000033	24	0·13	0·053013 ± 0·000038	329·4	2·8
Stein_8	136	0·000178	26	0·12	0·052976 ± 0·000048	327·8	3·1
Stein_10	101	0·000072	21	0·15	0·052985 ± 0·000076	328·2	4·0
Stein_11	57	0·000035	16	0·20	0·052900 ± 0·000097	324·5	4·8
Weighted av.						**328·1**	**1·7**

[1]Number of measured $^{207}Pb/^{206}Pb$ isotope ratios per grain.
[2]Model ratio calculated from $^{208}Pb^*/^{206}Pb^*$ ratio and age of the sample.
[3] indicates radiogenic lead.
[4]Error for each grain calculated according to the formula $\sqrt{(2\sigma/\sqrt{n})^2 + \Delta f^2}$, where n is the number of measured $^{207}Pb/^{206}Pb$ isotope ratios, 2σ is the 2σ standard deviation of the Gaussian frequency distribution function and Δf is an assumed uncertainty of the measured $^{207}Pb/^{206}Pb$ ratio of 0·1%.

Fig. 3. Cathodoluminescence (CL) images of representative zircon populations from granites of the Bavarian Forest: (a–d) Bavarian Terrane; (e–n) Ostrong Terrane. Scale bar represents 100 μm. Alternating change in luminescence colours, seen in most of the photographs, reflects variations in trace element contents (oscillatory growth zoning). In general, the intensity of luminosity in zircon crystals depends on the degree of metamictization and structural composition and usually differs between high-U (darker zones) and low-U parts (paler or brighter zones) (see also Corfu *et al.*, 2003).

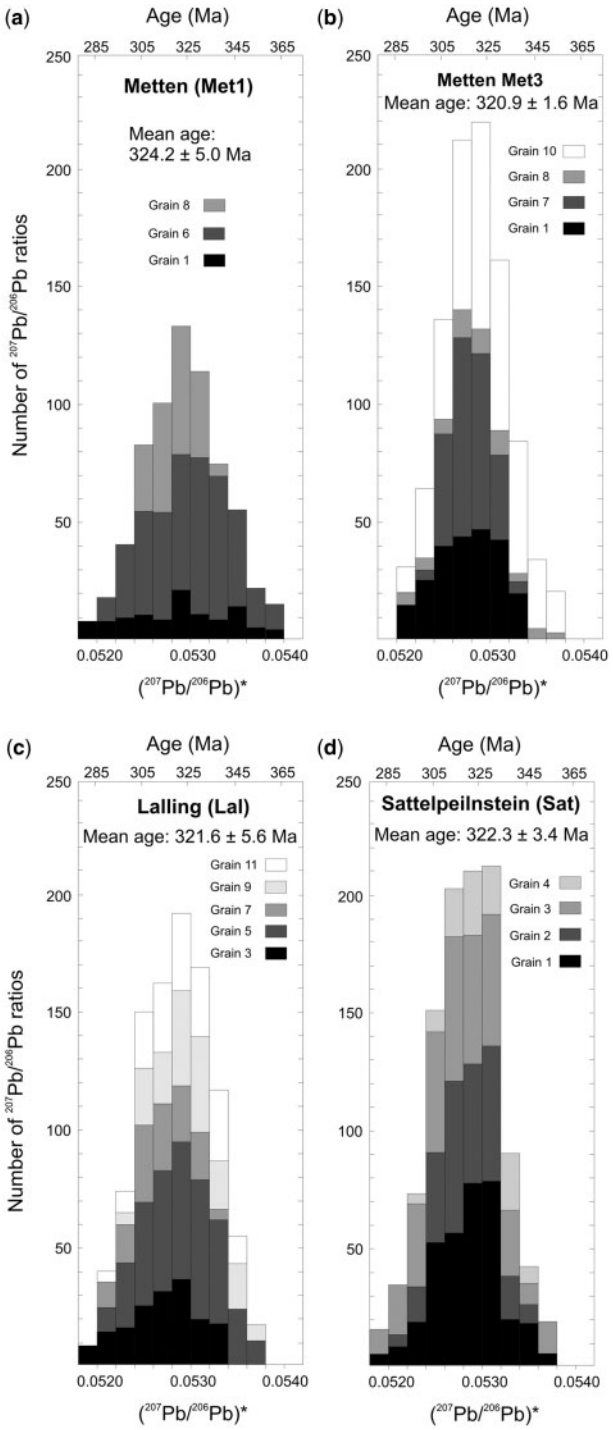

Fig. 4. Histograms showing the distribution of radiogenic $^{207}Pb/^{206}Pb$ ratios obtained from evaporation of zircons from granites of the Bavarian Terrane: (a, b) Metten; (c) Lalling; (d) Sattelpeilstein.

concentric zones were partly dissolved and replaced by darker zircon domains probably during late or post-magmatic stages (Fig. 3e). CL images also reveal that some grains contain cores of older magmatic zircons. Some of the cores can show well-developed pre-magmatic oscillatory zonation. In other grains (e.g. Fig. 3n, grains 2 and 3), zonation within the core is not concentric with respect to the external morphology of the grain, clearly indicating that older (i.e. inherited) grains were resorbed in the magma and subsequently overgrown by a new magmatic rim.

Four zircons from a sample of Miltach Granite (Mi) were vaporized and gave $^{207}Pb/^{206}Pb$ ages between 319 and 327 Ma, with a weighted mean age of 321·8 ± 3·7 Ma (Fig. 5a). Pre-magmatic zircon material was not detected in zircons from this sample. Zircon grains from the Arnbruck Granite show lead isotopic heterogeneity and yield $^{207}Pb/^{206}Pb$ minimum ages for the pre-magmatic zircon component around *c.* 335 Ma, 350 Ma and 410 Ma. Meaningful data with constant $^{207}Pb/^{206}Pb$ ratios for different temperature steps that are relevant for the determination of the crystallization age were obtained from only two grains. Both grains yield ages of *c.* 325 Ma and the mean age is 325 ± 2·1 Ma (Fig. 5b). After solidification, the Arnbruck Granite was cross-cut by the Runding Fault (Fig. 1). This resulted in a solid-state overprint of the granite, and the age data demonstrate that this tectonic disruption, which did not cause lateral displacement, was younger than 325 Ma.

From the Finsterau I Granite (sample Fin I) four grains yield virtually identical $^{207}Pb/^{206}Pb$ ages of *c.* 325 Ma, one grain gives an age of *c.* 329 Ma, and the weighted mean age of all five grains of 325·9 ± 1·9 Ma (Fig. 5c) is regarded as the time of crystallization for this granite. Three grains from sample Fin I were marked by slightly older age components between *c.* 340 and 350 Ma. Zircons with similar apparent ages, which might have been predominantly formed during the Variscan orogeny, were encountered in the Haidmühle and the Haidel Granites (see below). In the sample from Finsterau II (Fin II) we did not find evidence for zircon inheritance. Six analyses of zircons from this sample yielded $^{207}Pb/^{206}Pb$ ages between 321 and 327 Ma. The ages agree within analytical uncertainty and yield a weighted average age of 324·1 ± 1·8 Ma (Fig. 5d).

Zircon grains from Lusen sample Lu1 yield a range of old apparent $^{207}Pb/^{206}Pb$ ages and it seems that this zircon population is dominated by inheritance. Only one grain from this sample gave a Carboniferous age of 323·1 ± 3·5 Ma (Fig. 5e). Four analyses from sample Lu2 yielded homogeneous Pb-isotope compositions for different temperature steps and their total grain $^{207}Pb/^{206}Pb$ ages range between 320 and 328 Ma. The weighted mean of these four grains is 324·9 ± 3·5 Ma (Fig. 5f). One grain from sample Lu2 yields an older age of *c.* 340 Ma, which appears to have been derived from admixture of a pre-magmatic zircon domain.

Three zircon grains from a sample of the Dreisessel Granite yield well-defined $^{207}Pb/^{206}Pb$ ages of *c.* 327 Ma, which are identical within error, yielding a mean age of 327·1 ± 1·9 Ma (Fig. 6a). Notably, none of the grains show

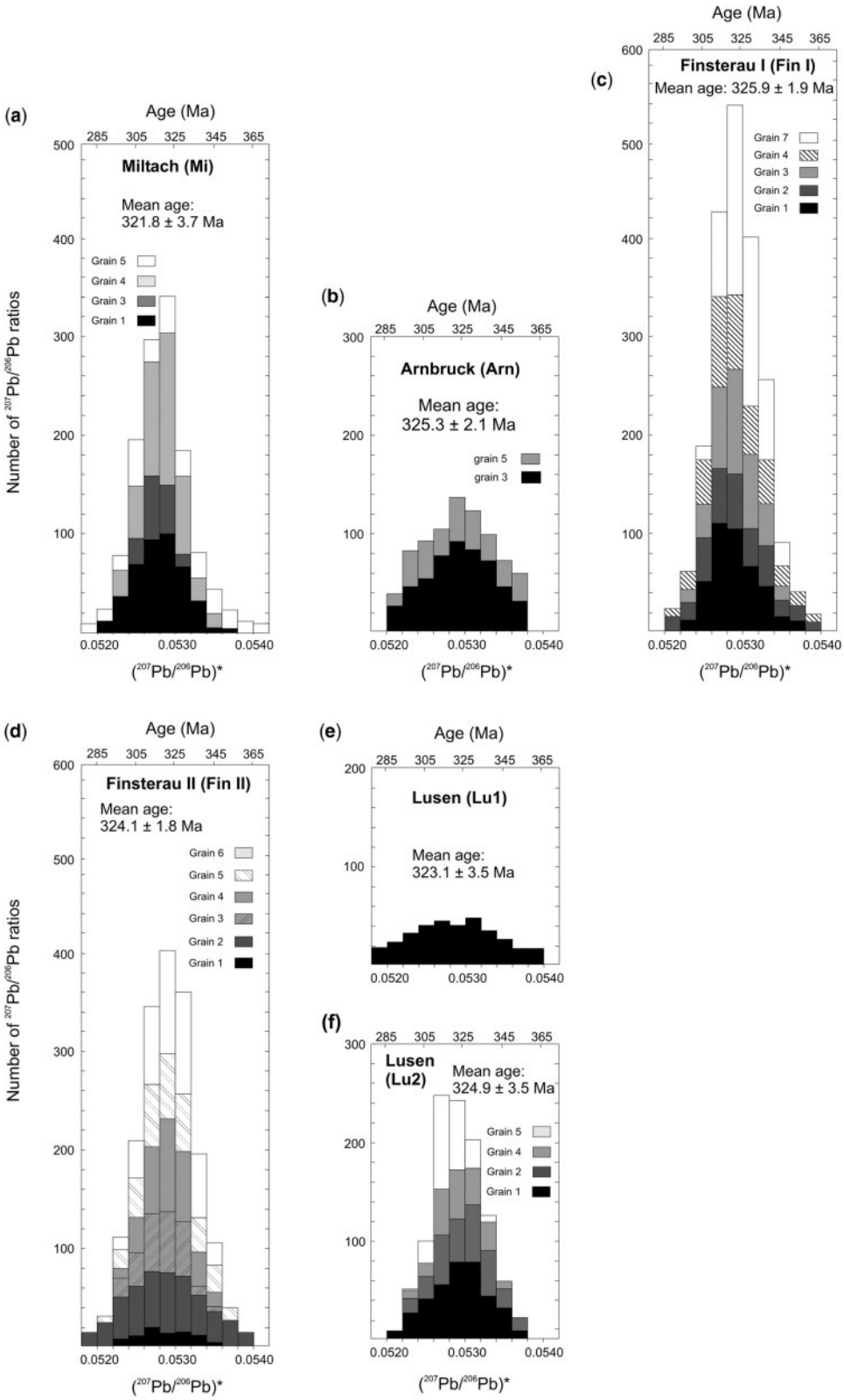

Fig. 5. Histograms showing the distribution of radiogenic $^{207}Pb/^{206}Pb$ ratios obtained from evaporation of zircons from granites of the Ostrong Terrane: (a) Miltach; (b) Arnbruck; (c) Finsterau I; (d) Finsterau II; (e, f) Lusen.

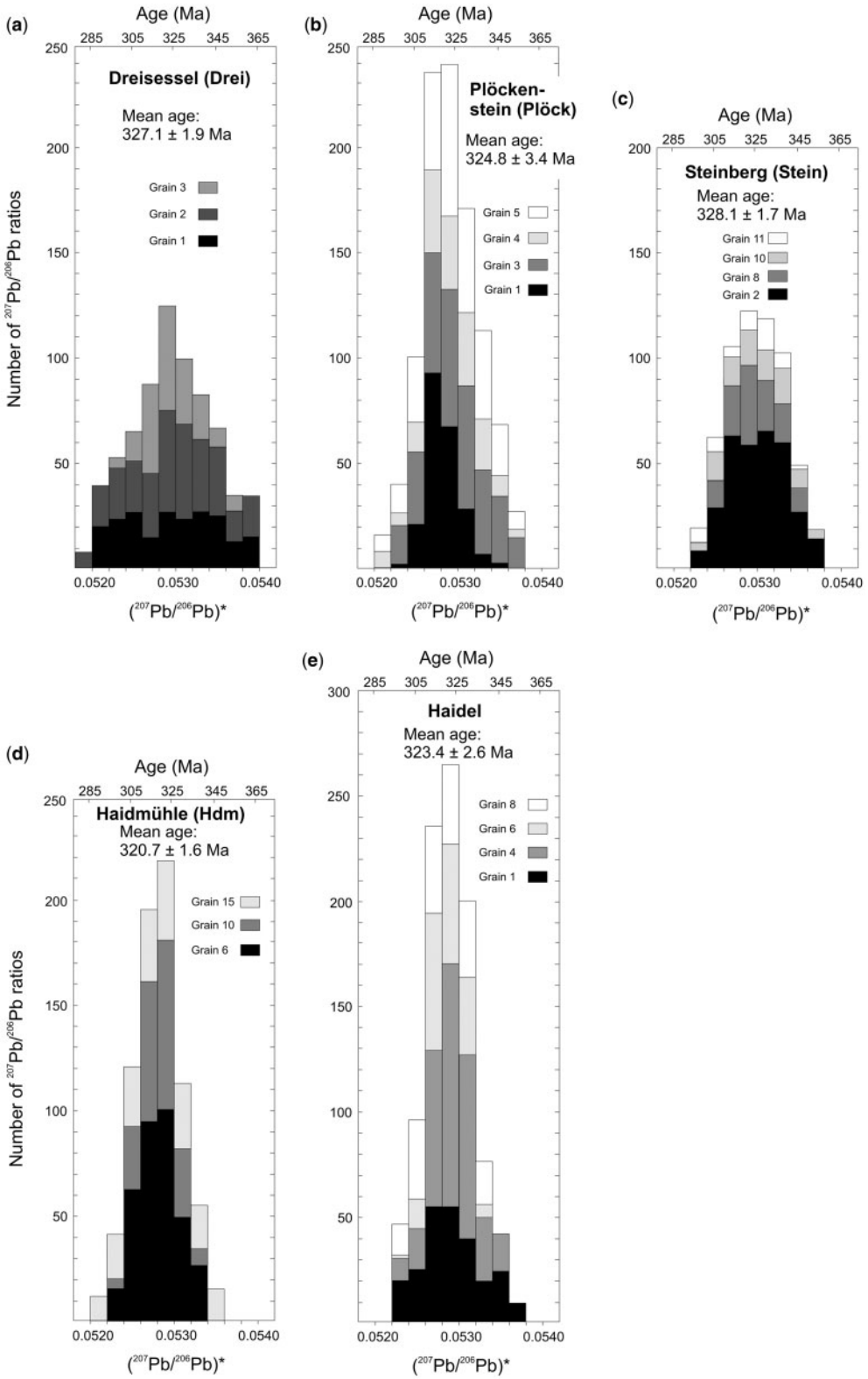

Fig. 6. Histograms showing the distribution of radiogenic $^{207}Pb/^{206}Pb$ ratios obtained from evaporation of zircons from granites of the Ostrong Terrane: (a) Dreisessel; (b) Plöckenstein; (c) Steinberg; (d) Haidmühle; (e) Haidel.

evidence for existence of a pre-magmatic zircon component. Four grains from a sample of the Plöckenstein Granite yield $^{207}Pb/^{206}Pb$ ages between 321 and 328 Ma (Fig. 6b), and the mean age of $324{\cdot}8 \pm 3{\cdot}4$ Ma is interpreted as the crystallization age of the Plöckenstein Granite. There is little evidence in the data for inheritance, as only one zircon yields a slightly older apparent $^{207}Pb/^{206}Pb$ age of *c.* 335 Ma. Four grains from the Steinberg Granite yielded homogeneous Pb-isotope compositions for different heating steps and their ages vary between 325 and 329 Ma, resulting in an average age of $328{\cdot}1 \pm 1{\cdot}7$ Ma (Fig. 6c). Heterogeneous $^{207}Pb/^{206}Pb$ ratios were measured in five grains and the highest temperature step, which can be regarded as the closest approximation to the minimum age of the inherited zircon component, gave apparent ages of *c.* 340 Ma, 370 Ma, 460 Ma and 650 Ma. The $^{207}Pb/^{206}Pb$ ages of three grains from the Haidmühle Granite are identical within error, yielding a mean age of $320{\cdot}7 \pm 1{\cdot}6$ Ma (Fig. 6d) that is interpreted as the magmatic crystallization age of the Haidmühle Granite. Zircons with apparent $^{207}Pb/^{206}Pb$ ages between 340 and 350 Ma were frequently encountered in this granite. In two other grains from the Haidmühle Granite, apparent ages of *c.* 370 Ma and *c.* 630 Ma were measured in the highest temperature steps. Of the zircons selected for Pb-evaporation analyses from the Haidel Granite, four grains yield consistent ages between 321 and 325 Ma, with a mean age of $323{\cdot}4 \pm 2{\cdot}6$ Ma (Fig. 6e). Two crystals give older apparent ages of *c.* 500 Ma and *c.* 670 Ma for the high-temperature evaporation steps. These data suggest a contribution from older (pan-African?) crust. Again, two other crystals yield slightly older apparent ages between *c.* 340 and *c.* 350 Ma similar to those found in the Haidmühle Granite.

Implications from geochronology

Despite the complexity of the Pb–Pb systematics encountered in numerous zircon grains from granites within the Bavarian Forest, the Pb–Pb evaporation data on magmatic zircons (i.e. those free of older inheritance) put important constraints on the chronology of pluton emplacement. Concerning the age data of purely magmatic zircon grains (Table 2), there seems to be a broad consistency in emplacement age between the various granites. Single-zircon $^{207}Pb/^{206}Pb$ evaporation ages of the granites investigated in this study range from 328 to 321 Ma in the Ostrong Terrane and from 324 to 321 Ma in the Bavarian Terrane. Clear regional age differences are virtually lacking. U–Pb and Pb–Pb zircon ages as young as 316–312 Ma have been reported for the Saldenburg and Eberhardsreuth intrusions from the composite Fürstenstein Pluton (Chen & Siebel, 2004), and these results reveal a younger, late Variscan intrusive event restricted to the southeastern part of the Bavarian Terrane. However, from the current geochronological dataset it is apparent that the majority of the granites intruded within a time span of less than 10 Myr, and this favours the interpretation that melting was initiated by a large regional heat flow event. The new data show that melt production and crustal high-temperature–low-pressure metamorphism in the Bavarian Forest were synchronous processes.

Relics of pre-magmatic (inherited) zircon components were detected in most of the investigated samples. In those zircon grains apparent ages between 340 and 350 Ma were most abundantly observed, particularly in granites from the Ostrong Terrane. This corresponds to the age of Moldanubian granulite metamorphism (e.g. Kröner *et al.*, 2000; Janoušek *et al.*, 2004) and several large granulite bodies of South Bohemia occur NE of the Dreisessel–Plöckenstein Pluton, close to our study area. Recently, Finger *et al.* (2007) reported evidence for earlier high-temperature–low-pressure metamorphism at 330–345 Ma in the southwestern Moldanubian sector. Taking the evidence from these studies, some of the pre-magmatic zircons found in the granites could have been derived from Early Carboniferous metamorphic rocks.

The analysed zircons from all the Bavarian granites show low Th/U signatures (from 0·02 to 0·41) with an average value of 0·135 (Table 2). No difference in Th/U between granites from the Bavarian and Ostrong Terranes could be found. The Th/U ratios tend to be distinctly less than the commonly quoted ratios of >0·5 for igneous zircons (Hoskin & Schaltegger, 2003). However, U/Th ratios in zircons from felsic granitic rocks are lower than in more mafic igneous rocks and are in the range of 0·11–1·0 (Ahrens *et al.*, 1967, fig. 1). Very low U/Th ratios are a common feature of differentiated S-type granites and have been reported for many magmatic zircons from granites of the Upper Palatinate Forest (Siebel *et al.*, 2003).

Regional geochemical comparison

Whole-rock geochemical and Nd–Sr isotope data from the samples investigated during this study are presented in Table 1. A comprehensive geochemical and isotopic dataset is now available for granites to the SW and NE of the Pfahl Zone, and in the following discussion we aim to compare the compositional features of the granites from these two regions. Literature data from the Bavarian Terrane, in addition to the data presented in Table 1, are from Chen & Siebel (2004) for the Fürstenstein Pluton, Siebel et al. (2006*a* and Siebel *et al.* in preparation) for granites from the Regensburg Forest and Siebel *et al.* (2006*b*) for the Rinchnach and Patersdorf Granites. The latter are closely linked with the Pfahl Zone (Fig. 1). The Patersdorf Granite occurs on both sides of this shear zone and the Rinchnach Granite immediately at its northern side. Both granites have geochemical affinities to the granites SW of the Pfahl Zone and in the following geochemical characterization they will be included in the group of the Bavarian Terrane granites.

Geochemical and Nd–Sr isotopic compositions of the major granite units are also established from studies in western Bohemia and the Southern Palatinate Forest. Data from these regions, which comprise the northward extension of the Ostrong Terrane (Fiala *et al.*, 1995; Finger *et al.*, 2007), come from the Rozvadov Pluton in Western Bohemia (Siebel *et al.*, 1999) and from the Southern Palatinate Forest (Neunburg Granite, Oberviechtach Granite) (Chen *et al.*, 2003). The dataset (Table 1 and literature data) comprises 27 granite samples from 14 intrusions from the Bavarian Terrane and 25 samples from 15 intrusions within the Ostrong Terrane.

Synthesis of the data shows that granites from the Bavarian and the Ostrong Terranes have distinctive geochemical characteristics (Fig. 7). According to the QAP classification, almost all samples plot in the granite field and only few can be classified as granodiorite (Fig. 7a). The other diagrams in Fig. 7 illustrate some fundamental chemical differences between these granites. The granites of the Bavarian Terrane are weakly peraluminous (aluminum saturation index, expressed as molar $Al_2O_3/(K_2O + Na_2O + CaO)$, A/CNK, from 1·0 to 1·2) whereas the granites within the Ostrong Terrane are strongly peraluminous with A/CNK values between 1·1 and 1·35 (Fig. 7b). According to the MALI classification ($Na_2O + K_2O - CaO$ vs silica) proposed by Frost *et al.* (2001), most granites plot in the calc-alkalic and alkali-calcic fields and the majority of granites from the Ostrong Terrane fit the compositional range of peraluminous leucogranites (Fig. 7c). Potassium exceeds sodium in most samples with large variation in K/Ca ratio (Fig. 7d). For the given dataset, Ca is a more useful discriminator than silica (Fig. 7e) and, in the remaining diagrams of Fig. 7, this is illustrated by plots of major and trace elements vs CaO. Calcium concentration is higher in the granites from the Bavarian Terrane. At the same time, these rocks are higher in other mafic elements (Ti–Fe–Mg) and lower in P (not shown) and less enriched in silica compared with those from the Ostrong Terrane. Amongst the trace elements, the Ca-rich granites contain higher concentrations of Y (Fig. 7j). The Ce/Y ratio, which can serve as an indicator of the fractionation between light and heavy rare earth elements, is low in the granites from the Bavarian Terrane but reaches higher values in granites from the Ostrong Terrane (Fig. 7k). The same relationship is found for the Rb/Sr ratios (Fig. 7l), reflecting a higher degree of differentiation of the granites from the Ostrong Terrane. From the diagrams shown in Fig. 7 there appears to be a fairly clear geochemical discrimination between high Ca–Sr–Y granites of the Bavarian Terrane and low Ca–Sr–Y granites of the Ostrong Terrane. As the only significant exception, the Finsterau I Granite has geochemical features more akin to the granites from the Bavarian Terrane (see also Table 1).

The Nd and Sr isotope compositions are plotted in Fig. 8. Recalculation of the Nd-isotope data to the emplacement age reveals that the Nd-isotope ratios (εNd values) of the high Ca–Sr–Y granites are higher (−3 to −7) than the range shown by the low Ca–Sr–Y granites (−5 to −9) (Fig. 8a). Accordingly, the initial Sr isotope ratios are less radiogenic in the high Ca–Sr–Y granites (0·705–0·710) and more radiogenic in the low Ca–Sr–Y granites (0·707–0·730) (Fig. 8b).

DISCUSSION AND IMPLICATIONS

The geochemical evidence presented in the previous section suggests different melting conditions or different source contributions for the granites NE and SW of the Pfahl Zone. The higher Ca and Sr contents of the granites from the Bavarian Terrane could simply be a reflection of a greater amount of plagioclase in their source material. In addition, these rocks require a garnet-free source to explain the low Ce/Y ratios and the high Y concentrations. During production of the low Ca–Sr–Y granites of the Ostrong Terrane, either melting of plagioclase was suppressed or the source was depleted in this mineral. Fractionation of plagioclase would result in depletion of Ca but also of Al; however, depletion of Al is not observed in the dataset (Fig. 7h). Melt extraction from a metapelite source in the presence of residual garnet would be a suitable process for the generation of these rocks. Because Ca and Sr are compatible elements in plagioclase and Y is a compatible trace element in apatite and zircon, the predominance of high Ca–Sr–Y granites in the Bavarian Terrane could reflect some accumulation of these early magmatic minerals supporting a cumulative nature of the magmatic rocks SW of the Pfahl Zone (F. Finger, personal communication). Cumulative magmatic rocks are typically exposed in deeper crustal levels and this is in line with the highly anatectic character of the Bavarian Terrane.

The isotope data give support to the assumption that the sources for the Bavarian granites that intruded the Bavarian Terrane were not identical to the sources for those that intruded the Ostrong Terrane (Fig. 8). Thus a tentative interpretation can be made that the basement must be of different type for the two terranes, with the Pfahl Shear Zone defining a terrane boundary (Fig. 9).

A zonation in granite composition can also be traced on the Austrian side of the Moldanubian sector: (1) I-type granites (so-called Schlieren granites) are dominant south of the Pfahl Zone in the Mühl Zone sector, which is the prolongation of the Bavarian Terrane into Austria; (2) S-type granites (Eisgarn type granite) are dominant north of the Pfahl Zone (e.g. Frasl & Finger, 1991; Finger & Clemens, 1995). This zonation was ascribed by Frasl & Finger (1991) to reflect different composition of the pre-anatextic crust or different crustal levels. Thus it appears

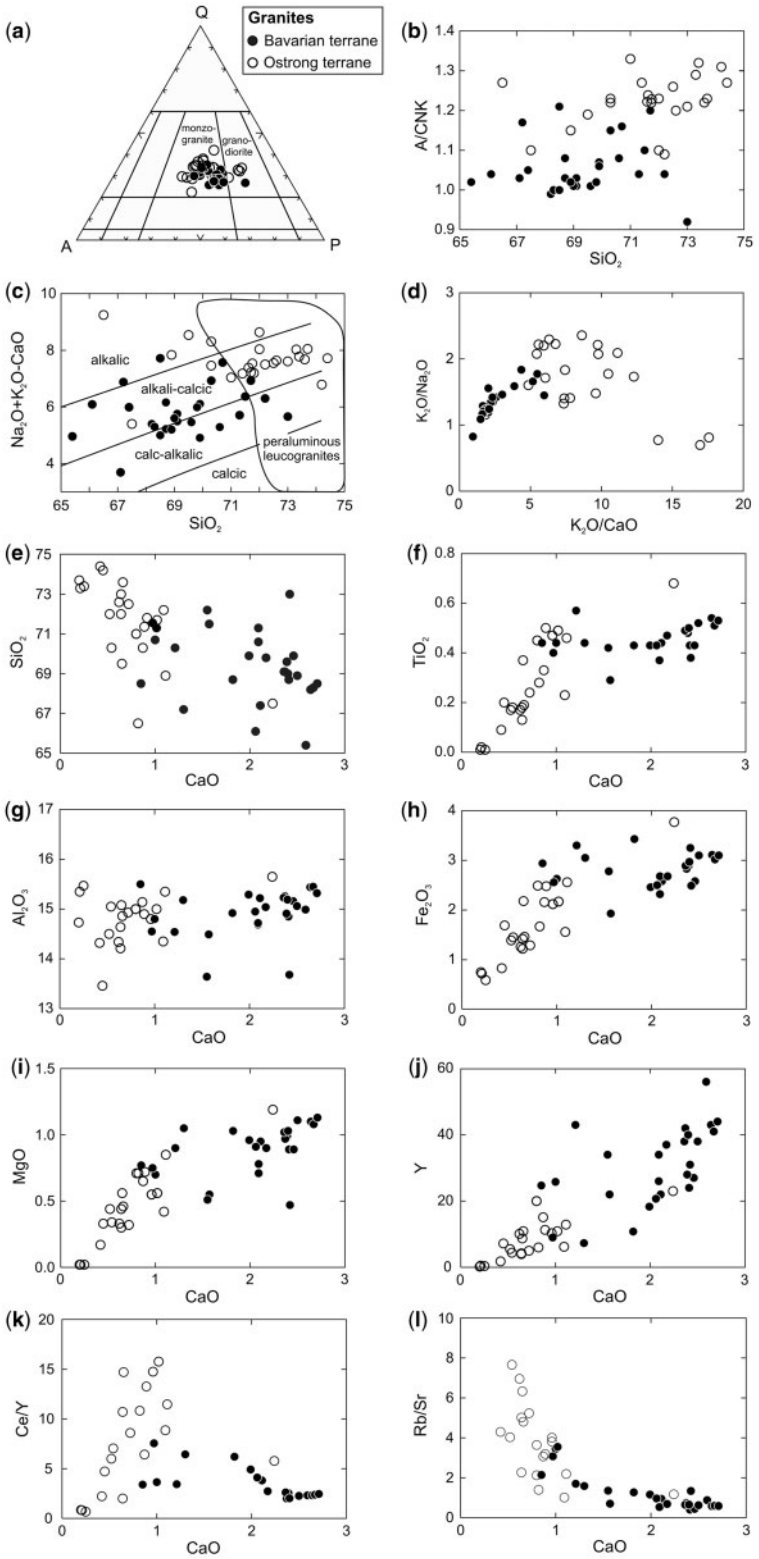

Fig. 7. (a) Classification of the granites of the Bavarian Forest and adjacent areas on the QAP (quartz–alkali-feldspar–plagioclase) diagram (Streckeisen, 1976); (b) aluminum saturation index [ASI, molar $Al_2O_3/(K_2O + Na_2O + CaO)$] vs silica diagram; (c) modified alkali–lime index (MALI) vs silica diagram (Frost *et al.*, 2001); (d) K_2O/Na_2O vs K_2O/CaO diagram; (e–l) variation of selected major and trace elements with CaO (wt %).

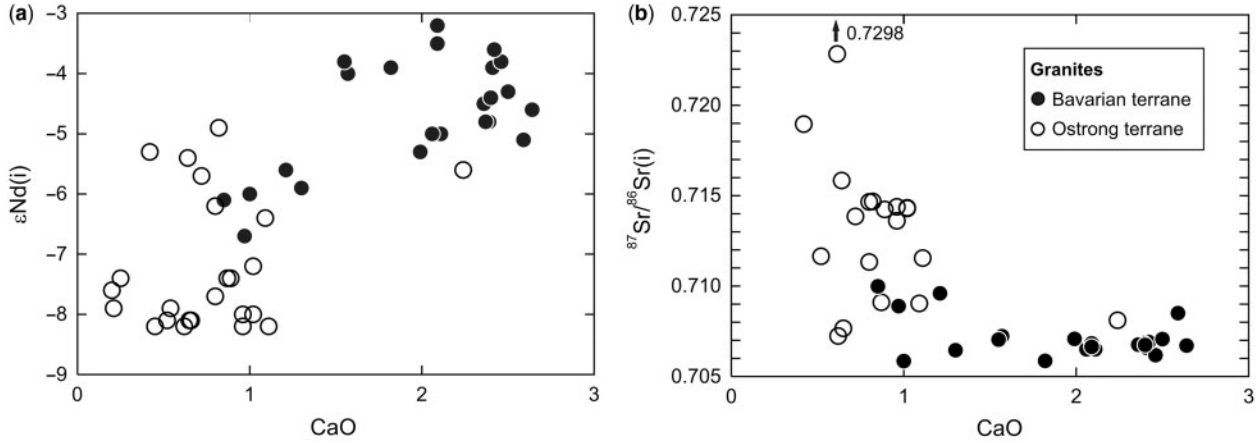

Fig. 8. Plot of (a) εNd value and (b) $^{87}Sr/^{86}Sr$ ratio (recalculated to the age of granite emplacement) vs CaO (wt %).

that this striking spatial zonation is a general feature of the southern Moldanubian sector.

Figure 10 shows that the compositions of the granites are largely consistent with melts derived from experimental partial melting of different metapelite compositions (Patiño-Douce, 1999). These diagrams also suggest that amphibolites and meta-greywackes are less suitable sources for the majority of the granites. Pelitic or semi-pelitic metasedimentary gneisses like the outcropping garnet- and cordierite-bearing rocks of the Ostrong Terrane, which may continue at greater depth, could be regarded as potential sources of the granites within this unit. Such a source would yield sufficient quantities of melt of peraluminous composition (e.g. Koester *et al.*, 2002).

We have argued elsewhere (Siebel *et al.*, 2006*a*) that the granites of the Bavarian Terrane (i.e. Regensburg Forest) were probably derived from more mafic protoliths than the now exposed diatexites of this area. Some involvement of mantle-derived magma was postulated in the petrogenesis of the the Saldenburg and Tittling Granites of the Fürstenstein Pluton (Chen & Siebel, 2004). It is a general observation that small dioritic bodies are more frequently found SE of the Pfahl Zone. Thus it might be argued that additional input of mantle-derived material to the crust of the Bavarian Terrane has played a role in granitoid magma genesis. However, there is little field evidence to suggest that these granites are the products of hybridization between crustal- and mantle-derived magmas. For most of the Bavarian Terrane granites no clear correlation is visible in the εNd vs Ca diagram (Fig. 8a). This argues against two-component mixing between mafic (mantle) and felsic (diatexite) components. In addition, the preponderance of granitic rocks over dioritic rocks in the Bavarian Forest is not compatible with the involvement of larger volumes of mantle-derived magma during granite petrogenesis. For a conclusive judgement, it has to be verified in more detail whether the Moldanubian basement rocks have the isotope composition required to be a potential source.

Crustal melting demands a heat source and, given the synchronism between magmatism and metamorphism, it is likely that metamorphism set the stage for the creation of a melt flow network within the crust, and this aided melt extraction, granite formation and crustal anatexis. It was previously pointed out by Finger & Clemens (1995) that in the Mühl Zone, intrusions of voluminous granites such as the Weinsberg Granite supplied heat and caused large-scale anatexis in neighbouring rocks. Ultimately, this late Variscan 'hot crustal phase' could have been triggered by radiogenic intracrustal heating (Gerdes *et al.*, 2000) or delamination of mantle lithosphere (Henk *et al.*, 2000; Finger *et al.*, 2007).

CONCLUSIONS

Single-zircon Pb-evaporation analyses show that granite formation in the southwestern Moldanubian Sector of the Bohemian Massif was synchronous with the peak of high-temperature–low-pressure metamorphism. The $^{207}Pb/^{206}Pb$ evaporation ages of 14 granite intrusive rocks from the Bavarian Forest are consistent with a short episode of crustal melting between 328 and 321 Ma. Overall, this study demonstrates the feasibility of using the Pb-evaporation method to establish the detailed geochronology of S-type granites despite complexities resulting from inherited zircon material.

Taking bulk-rock geochemical and isotopic characteristics into account, it now appears that the granites from the Bavarian Terrane and the Ostrong Terrane define two distinct granite types, which formed at about the same time but from different source materials. The presence of high- and low-Ca–Sr–Y granites with distinct Nd–Sr signatures confirms earlier suggestions that the Pfahl

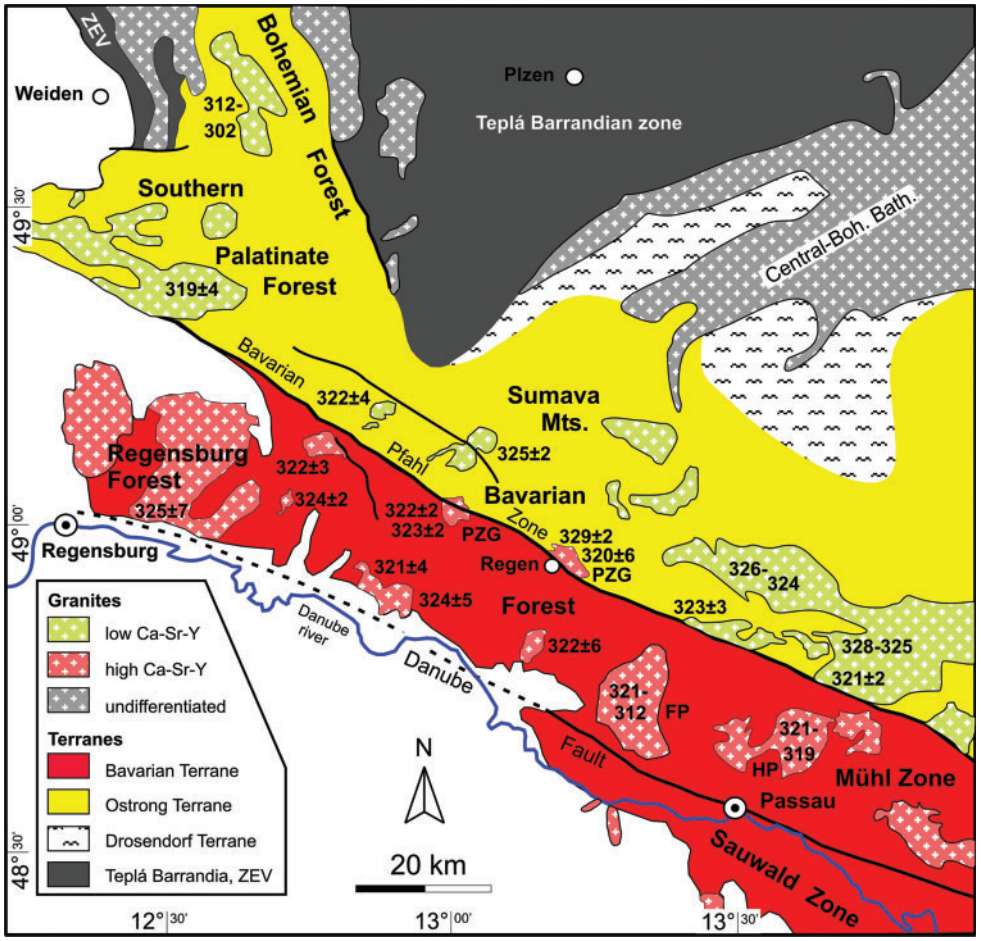

Fig. 9. Tentative distribution of high Ca–Sr–Y and low Ca–Sr–Y granites in the western part of Moldanubian sector. Terrane definition according to Fiala *et al.* (1995). Numbers denote crystallization ages (in million years) of plutons as determined here and in earlier studies: Southern Palatinate Forest (Chen *et al.*, 2003), Regensburg Forest (Siebel *et al.*, 2006*a* Siebel *et al.* in preparation), Fürstenstein Pluton, FP (Chen & Siebel, 2004), Pfahl Zone granites, PZG (Siebel *et al.*, 2006*b*), Hauzenberg Pluton, HP (Klein *et al.*, 2008), Bohemian Forest (Rozvadov Pluton) (Siebel *et al.*, 1999).

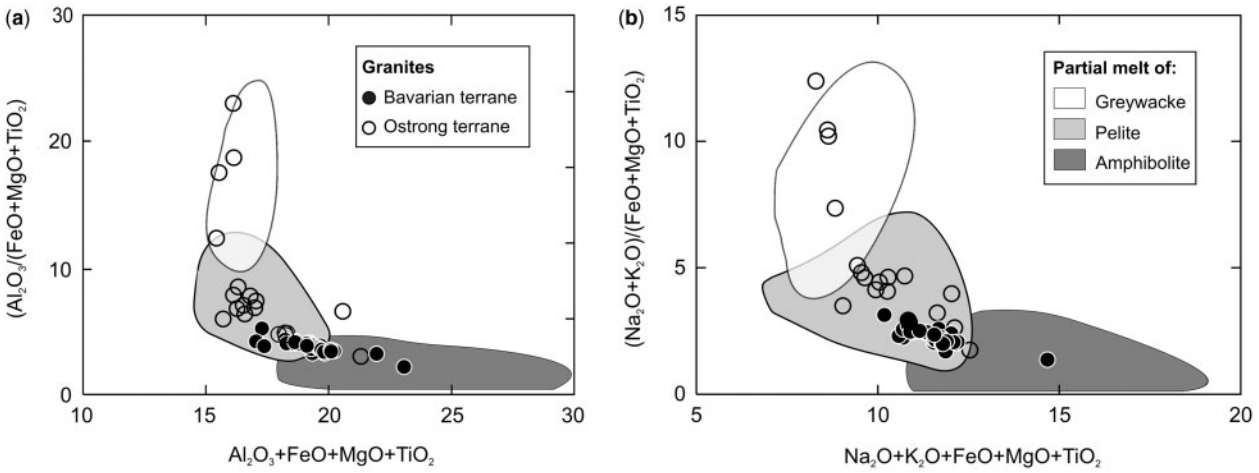

Fig. 10. Geochemical composition of granites in major oxide diagrams. (a) $Al_2O_3/(FeO+MgO+TiO_2)$ vs $Al_2O_3+FeO+MgO+TiO_2$; (b) $(Na_2O+K_2O)/(FeO+MgO+TiO_2)$ vs $Na_2O+K_2O+FeO+MgO+TiO_2$. Outlined fields denote compositional fields of experimental melts derived from partial melting of felsic pelites, metagreywackes and amphibolites (Patiño-Douce, 1999).

Shear Zone is a terrane boundary that has juxtaposed two compositionally distinct Variscan basement units (Fig. 9). More work is required to ascertain the compositional differences between the two units.

ACKNOWLEDGEMENTS

We thank G. Bartholomä for zircon separation, Ch. Dekant and H. Schulz for their assistance in providing CL images, and H. Taubald for help during XRF analyses. Financial support from the Bavarian Environment Agency is gratefully acknowledged.

REFERENCES

Affaton, P., Kröner, A. & Seddoh, K. F. (2000). Pan-African granulite formation in the Kabye massif of northern Togo (West Africa): Pb–Pb zircon ages. *International Journal of Earth Sciences* **88**, 778–790.

Ahrens, L. H., Cherry, R. D. & Erlank, A. J. (1967). Observations on the Th–U relationship in zircons from granitic rocks and from kimberlites. *Geochimica et Cosmochimica Acta* **31**, 2379–2387.

Bauberger, W. (1981). Zur Geologie des Nationalparks Bayerischer Wald. *Der Aufschluss* **31**, 15–32.

Blížkovský, M. & Novotný, A. (1982). *Gravity map of the Bohemian Massif*. Brno: Geofyzika.

Breiter, K. & Koller, F. (2005). New interesting types of granitoids in the Three-corner-country (Dreiländereck) of Austria, Czech Republic and Germany. *Mitteilungen der Österreichischen Mineralogischen Gesellschaft* **151**, 33 .

Breiter, K., Koller, F., Scharbert, S., Siebel, W., Škoda, R. & Frank, W. (2007). Two-mica granites of the Plechý (Plöckenstein) pluton in the triple-point area (Trojmezí, Dreiländereck) of Austria, the Czech Republic, and Germany. *Jahrbuch der Geologischen Bundesanstalt Wien* **147**, 527–544.

Chapman, H. J. & Roddick, J. C. (1994). Kinetics of Pb release during the zircon evaporation technique. *Earth and Planetary Science Letters* **121**, 601–611.

Chen, F. & Siebel, W. (2004). Zircon and titanite geochronology of the Fürstenstein granite massif, Bavarian Forest, NW Bohemian Massif: Pulses of late Variscan magmatic activity. *European Journal of Mineralogy* **16**, 777–788.

Chen, F., Siebel, W. & Satir, M. (2002). Zircon U–Pb and Pb-isotope fractionation during stepwise HF-acid leaching and chronological implications. *Chemical Geology* **191**, 155–164.

Chen, F., Siebel, W. & Satir, M. (2003). Geochemical and isotopic composition and inherited zircon ages as evidence for lower crustal origin of two Variscan S-type granites in the NW Bohemian Massif. *International Journal of Earth Sciences* **92**, 173–184.

Cocherie, A., Guerrot, C. & Rossi, P. (1992). Single-zircon dating by step-wise Pb evaporation: comparison with other geochronological techniques applied to the Hercynian granites of Corsica, France. *Chemical Geology* **101**, 131–141.

Connelly, J. N. (2000). Degree of preservation of igneous zonation in zircon as a signpost for concordancy in U/Pb geochronology. *Chemical Geology* **172**, 25–39.

Corfu, F., Hanchar, J. M., Hoskin, P. W. O. & Kinny, P. (2003). Atlas of zircon textures. In: Hanchar, J. M. & Hoskin, P. W. O. (eds) *Zircon. Mineralogical Society of America and Geochemical Society, Reviews in Mineralogy and Geochemistry* **53**, 469–500.

Dollinger, U. (1967). Das Hauzenberger Granitmassiv und seine Umrahmung. *Geologica Bavarica* **58**, 145–172.

Dougherty-Page, J. S. & Bartlett, J. M. (1999). New analytical procedures to increase the resolution of zircon geochronology by the evaporation technique. *Chemical Geology* **153**, 227–240.

Fiala, J., Fuchs, G. & Wendt, J. I. (1995). Stratigraphy of the Moldanubian zone. In: Dallmeyer, R. D., Franke, W. & Weber, K. (eds) *Pre-Permian Geology of Central and Eastern Europe*. Berlin: Springer, pp. 417–428.

Finger, F. & Clemens, J. D. (1995). Migmatization and 'secondary' granitic magmas: effects of emplacement and crystallization of 'primary' granitoids in Southern Bohemia, Austria. *Contributions to Mineralogy and Petrology* **120**, 311–326.

Finger, F., Gerdes, A., Janoušek, V., René, M. & Riegler, G. (2007). Resolving the Variscan evolution of the Moldanubian sector of the Bohemian Massif: the significance of the Bavarian and the Moravo-Moldanubian tectonometamorphic phases. *Journal of Geosciences* **52**, 9–28.

Frasl, G. & Finger, F. (1991). Geologisch-petrographische Exkursion in den österreichischen Teil des südböhmischen Batholiths. *Berichte der Deutschen Mineralogischen Gesellschaft* **3**(2), 23–40.

Frost, B. R., Barnes, C. G., Collins, W. J., Arculus, R. J., Ellis, D. J. & Frost, C. D. (2001). A geochemical classification of granitic rocks. *Journal of Petrology* **42**, 2033–2048.

Fuchs, G. (1976). Zur Entwicklung der Böhmischen Masse. *Jahrbuch der Geologischen Bundesanstalt* **119**, 45–61.

Gerdes, A., Wörner, G. & Henk, A. A. (2000). Post-collisional granite generation and HT–LP metamorphism by radiogenic heating: the Variscan South Bohemian Batholith. *Journal of the Geological Society, London* **157**, 577–587.

Görz, I., Bombach, K., Kroner, U. & Ivanov, K.S. (2004). Protolith and deformation age of the gneiss-plate of Kartali in the southern East Uralian Zone. *International Journal of Earth Sciences* **93**, 475–486.

Goldstein, S.L., O'Nions, R. K. & Hamilton, P. J. (1984). A Sm–Nd study of atmospheric dusts and particulates from major river systems. *Earth and Planetary Science Letters* **70**, 221–236.

Henk, A. A., von Blankenburg, F., Finger, F., Schaltegger, U. & Zulauf, G. (2000). Syn-convergent high-temperature metamorphism and magmatism in the Variscides: a discussion of potential heat sources. In: Franke, W., Haak, V., Oncken, O. & Tanner, D. (eds) *Orogenic Processes: Quantification and Modelling in the Variscan Belt. Geological Society, London, Special Publications* **179**, 387–399.

Holub, F. V., Klečka, M. & Matějka, D. (1995). Igneous activity. In: Dallmeyer, R. D., Franke, W. & Weber, K. (eds) *Pre-Permian Geology of Central and Eastern Europe*. Berlin: Springer, pp. 444–452.

Hoskin, P. W. O. & Schaltegger, U. (2003). The composition of zircon and igneous and metamorphic petrogenesis. In: Hanchar, J. M. & Hoskin, P. W. O. (eds) *Zircon. Mineralogical Society of America and Geochemical Society, Reviews in Mineralogy and Geochemistry* **53**, 27–62.

Jacobsen, K. & Wasserburg, G. J. (1980). Sm–Nd isotopic evolution of chondrites. *Earth and Planetary Science Letters* **50**, 139–155.

Janoušek, V., Finger, F., Roberts, M. P., Frýda, J., Pin, C. & Dolejš, D. (2004). Deciphering petrogenesis of deeply buried granites: whole-rock geochemical constraints on the origin of largely undepleted felsic granulites from the Moldanubian Zone of the Bohemian Massif. *Transactions of the Royal Society of Edinburgh, Earth Sciences* **95**, 141–159.

Kalt, A., Berger, A. & Blümel, P. (1999). Metamorphic evolution of cordierite-bearing migmatites of the Bayerische Wald (Variscan Belt, Germany). *Journal of Petrology* **40**, 601–627.

Kalt, A., Corfu, F. & Wijbrans, J. R. (2000). Time calibration of a *P–T* path from a Variscan high-temperature low-pressure metamorphic complex (Bayerische Wald, Germany), and the detection of inherited monazite. *Contributions to Mineralogy and Petrology* **138**, 143–163.

Karabinos, P. (1997). An evaluation of the single-grain zircon evaporation method in highly discordant samples. *Geochimica et Cosmochimica Acta* **61**, 2467–2474.

Klein, P., Kiehm, S., Siebel, W., Shang, C. K., Rohrmüller, J., Dörr, S. & Zulauf, G. (2008). Age and emplacement of late-Variscan granites of the western Bohemian Massif with main focus on the Hauzenberg granitoids. *Lithos* **102**, 478–507.

Klötzli, U. S. (1997). Single zircon evaporation thermal ionisation mass spectrometry: method and procedure. *Analyst* **122**, 1239–1248.

Klötzli, U. S. (1999). Th/U zonation in zircon derived from evaporation analysis: a model and its implications. *Chemical Geology* **158**, 325–333.

Kober, B. (1986). Whole-grain evaporation for $^{207}Pb/^{206}Pb$-age-investigations on single zircons using a double-filament thermal ion source. *Contributions to Mineralogy and Petrology* **93**, 482–490.

Kober, B. (1987). Single-zircon evaporation combined with Pb^{+} emitter-bedding for $^{207}Pb/^{206}Pb$-age investigations using thermal ion mass spectrometry, and implications to zirconology. *Contributions to Mineralogy and Petrology* **96**, 63–71.

Koester, E., Pawley, A. R., Fernandes, L. A. D., Porcher, C. C. & Soliani, E. (2002). Experimental melting of cordierite gneiss and the petrogenesis of syntranscurrent peraluminous granites in southern Brazil. *Journal of Petrology* **43**, 1595–1616.

Kröner, A., O'Brien, P. J., Nemchin, A. A. & Pidgeon, R. T. (2000). Zircon ages for high pressure granulites from South Bohemia, Czech Republic, and their connection to Carboniferous high temperature processes. *Contributions to Mineralogy and Petrology* **138**, 127–142.

Kröner, A., Jaeckel, P., Hegner, E. & Opletal, M. (2001). Single zircon ages and whole-rock Nd isotopic systematics of early Palaeozoic granitoid gneisses from the Czech and Polish Sudetes (Jizerské hory, Krkonoše Mountains and Orlice–Sněžník Complex). *International Journal of Earth Sciences* **90**, 304–324.

Liew, T. C. & Hofmann, A. W. (1988). Precambrian crustal components, plutonic associations, plate environment of the Hercynian Fold Belt of central Europe: Indications from a Nd and Sr isotopic study. *Contributions to Mineralogy and Petrology* **98**, 129–138.

Ludwig, K. R. (2003). *Isoplot/Ex, rev 3.00: A geochronological toolkit for Microsoft Excel. Berkeley Geochronology Center, Special Publications* **4**, 1–58.

Ott, W. D. (1988). *Geological map of Bavaria. Explanations to 1:25 000 sheet 7149 Freyung and 7148 Bischofsreut*. Munich: Geological Survey of Bavaria.

Ott, W. D. (1992). *Geological map of Bavaria. Explanations to 1:25 000 sheet 7248/49 Jandelsbrunn*. Munich: Geological Survey of Bavaria.

Patiño-Douce, A. E. (1999). What do experiments tell us about the relative contribution of crust and mantle to the origin of granitic magmas? In: Castro, A., Fernandez, C. & Vigneresse, J. L. (eds) *Understanding Granites: Integrating New and Classical Techniques Geological Society, London, Special Publications* **168**, 55–75.

Propach, G. (1989). The origin of a conformable Variscan granite in Bavaria—results of geochemical and geochronological investigations. In: Bonin, B. & Didier, J. (eds) *Magma crust interactions and evolution*. Athens: Theophrastus Publications, pp. 193–209.

Propach, G., Baumann, A., Schulz-Schmalschläger, M. & Grauert, B. (2000). Zircon and monazite U–Pb ages of Variscan granitoid rocks and gneiss in the Moldanubian zone of eastern Bavaria, Germany. *Neues Jahrbuch für Geologie und Paläontologie, Monatshefte* **2000**(6), 345–377.

Schreyer, W. (1967). Das Grundgebirge in der Umgebung von Deggendorf an der Donau. *Geologica Bavarica* **58**, 77–85.

Siebel, W., Breiter, K., Wendt, I., Höhndorf, A., Henjes-Kunst, F. & René, M. (1999). Petrogenesis of contrasting granitoid plutons in western Bohemia (Czech Republic). *Mineralogy and Petrology* **65**, 207–235.

Siebel, W., Chen, F. & Satir, M. (2003). Late Variscan magmatism revisited: new implications from Pb-evaporation zircon ages on the emplacement of redwitzites and granites in NE Bavaria. *International Journal of Earth Sciences* **92**, 36–53.

Siebel, W., Hann, H. P., Shang, C. K., Rohrmüller, J. & Chen, F. (2006*a*). Coeval late-Variscan emplacement of granitic rocks: an example from the Regensburger Wald, NE Bavaria. *Neues Jahrbuch für Mineralogie* **183**, 13–26.

Siebel, W., Thiel, M. & Chen, F. (2006*b*). Zircon geochronology and compositional record of late- to post-kinematic granitoids associated with the Bavarian Pfahl zone (Bavarian Forest). *Mineralogy and Petrology* **86**, 45–62.

Streckeisen, A. (1976). To each plutonic rock its proper name. *Earth-Science Reviews* **12**, 1–33.

Teipel, U., Eichhorn, R., Loth, G., Rohrmüller, J., Höll, R. & Kennedy, A. (2004). U–Pb SHRIMP and Nd isotopic data from the western Bohemian Massif (Bayerischer Wald, Germany): Implications for Upper Vendian and Lower Ordovician magmatism. *International Journal of Earth Sciences* **93**, 782–801.

Teipel, U., Galadí-Enríquez, E., Glaser, S., Krömer, E., Rohrmüller, J. (2008). Geological map of the Bavarian Forest 1:150 000. Bavarian Environment Agency, Augsburg.

Thiele, O. & Fuchs, G. (1965). *Übersichtskarte des Kristallins im westlichen Mühlviertel und im Sauwald, Oberösterreich*. Vienna: Geologische Bundesanstalt.

Verner, K., Žák, J., Pertoldová, J., Šrámek, J., Sedlák, J., Trubač, J. & Týcová, P. (2008). Magmatic history and geophysical signature of a post-collisional intrusive centre emplaced near a crustal-scale shear zone: the Plechý granite pluton (Moldanubian batholith, Bohemian Massif). *International Journal of Earth Sciences* **97**, 19–33.

Winchester, J. A., Pharaoh, T. C. & Verniers, J. (eds) (2002). *Palaeozoic Amalgamation of Central Europe. Geological Society, London, Special Publications* **201**, 352 pp.